

PHYSICAL REVIEW A

GENERAL PHYSICS

THIRD SERIES, VOLUME 29, NUMBER 3

MARCH 1984

Classification and supermultiplet structure of doubly excited states

C. D. Lin

Department of Physics, Kansas State University, Manhattan, Kansas 66506

(Received 21 July 1983)

Based upon the analysis of electron correlations in hyperspherical coordinates for arbitrary L , S , and π states, a classification scheme for all doubly excited states of two-electron atoms is presented. A new set of internal correlation quantum numbers, K , T , and A , are introduced. Here (K, T) describe angular correlations and $A = \pm 1, 0$ describes radial correlations. These quantum numbers are used to label the first-order wave functions which are approximated as $\Psi = F_\mu^n(R)\Phi_\mu(R; \Omega)$ in terms of hyperspherical coordinates. The channel index μ is $\mu \equiv |(K, T)_N^{A, 2S+1, L, \pi}\rangle$, where N is the dissociation limit of the channel. Rules for constructing the correlation diagram for channel potential $U_\mu(R)$ and the labeling of each channel are discussed. By comparing the rotation-averaged surface charge densities, it is shown that channels which have identical $(K, T)_N^{A, \pi}$ have isomorphic correlation patterns, irrespective of the overall L , S , and π . Such isomorphism is shown to be the underlying origin of the supermultiplet structure of intrashell doubly excited states. In fact, it is shown that such supermultiplet structures actually extend to *all* states which have $A = +1$ or -1 . A new Grotrian diagram for energy levels grouped according to $(K, T)^+$ and $(K, T)^-$ displays rotor-like structure. Such diagrams can easily reveal missing or misclassified levels. It is also shown that all $A = 0$ states are similar to singly excited states where for a given $(K, T)_N^0$, the triplet state always has a slightly lower energy than the singlet state. Approximate selection rules for photoabsorption and for e -H and e -He⁺ scatterings are discussed.

I. INTRODUCTION

Since the identification of doubly excited states¹ of He in 1963, it has been well established^{2,3} that these states cannot be adequately described in terms of the conventional independent-particle model. A new set of quantum numbers is desirable for the classification of these states. However, due to the lack of understanding of electron correlations for doubly excited states, such a scheme has not been available so far.

Over the last few years, partial understanding of electron correlations for doubly excited states has emerged gradually.⁴⁻⁶ In a series of articles,⁵ the author has investigated radial and angular correlations for S states of H⁻ and He. These correlations were analyzed by assuming quasiseparability of wave functions in hyperspherical coordinates. In Ref. 5(c), it was illustrated that these approximate quasiseparable wave functions agree very well with those obtained using the large-scale conventional configuration-interaction (CI) method. Thus the reliability of quasiseparability of wave functions in hyperspherical coordinates is well established and different channels were shown to exhibit striking differences in radial and angular correlations.

Attempts for classifying doubly excited states along different lines of approaches have also been made by several

other groups.⁷⁻¹¹ In particular, Herrick and Sinanoglu⁷ proposed doubly-excited-states-basis (DESB) functions to represent the first-order approximation of these states. The DESB functions are equivalent to approximate CI functions where only the intrashell correlations are included. In Ref. 6 it was shown that such DESB functions are, in general, lacking of sufficient radial correlation and for some states also lacking of sufficient angular correlation. Thus linear superpositions of DESB functions are needed, in general, in order to give a good description of doubly excited states.

Under the assumption of quasiseparability in hyperspherical coordinates, the wave functions are expressed as $F_\mu^n(R)\Phi_\mu(R; \Omega)$ where $R = (r_1^2 + r_2^2)^{1/2}$, $\Omega \equiv (\alpha, \hat{r}_1, \hat{r}_2)$, and $\alpha = \arctan(r_2/r_1)$. In this approximation, μ is the channel index, $\Phi_\mu(R; \Omega)$ is the channel function, and $F_\mu^n(R)$ is obtained by solving the one-dimensional radial equation from the channel potential $U_\mu(R)$. The channel function $\Phi_\mu(R; \Omega)$, which depends on R parametrically, contains all the information about electron correlations for states within that channel. The validity of quasiseparability for all values of R , as shown in our earlier works,⁵ also implies that the correlation pattern for a given channel is nearly invariant. However, until very recently, it has not been possible to relate the channel index μ to some apparent quantum numbers which also provide information

about electron correlations.

In a recent communication,¹² we reported a new classification scheme for all doubly excited states of two-electron atoms. Through the analysis of electron correlations, we propose a new set of quantum numbers which is to replace the quantum numbers used in the independent-particle model. According to the latter model, the two electrons within the LS coupling scheme are described by $n_1, l_1, n_2, l_2, L, S, \pi, M_L,$ and M_S , where n_i is the principal quantum number of electron i and the rest have their usual meanings. Since configuration mixings are quite strong for doubly excited states, the quantum numbers $n_1, l_1, n_2,$ and l_2 are no longer meaningful in identifying the states. Herrick and Sinanoglu⁷ considered the mixing of l_1 and l_2 pairs within a *fixed* n_1 and n_2 in their DESB functions and introduced two new quantum numbers, K and T , to replace l_1 and l_2 . As shown in Ref. 6, DESB functions do not incorporate radial correlation adequately and cannot be used as a first-order approximation for doubly excited states. Instead of the quantum numbers $n_1, n_2, K, T, L, S,$ and π used in the DESB functions, we propose that a first-order approximation of doubly excited state is given by $F_\mu^n(R)\Phi_\mu(R;\Omega)$, where the channel index $\mu \equiv \{N, (K, T)^A, L, S, \pi\}$. In other words, a given doubly excited state is represented by the set of quantum numbers $n, N, (K, T)^A, L, S,$ and π where n is the radial quantum number of the outer electron, N is the dissociation limit of the channel, and $(K, T)^A$ is the new set of *correlation quantum numbers*.

Our choices of K and T quantum numbers are identical to those used by Herrick and Sinanoglu.⁷ However, we do *not* associate K and T to DESB functions *directly*. Instead, they are used to label dipole states,¹³ i.e., the Stark states of the system when one electron is far away from the other. In the present context, K and T are used to describe angular correlations only. To account for radial correlation, we introduce $A = +1, -1,$ and 0 . For $A = +1$, we emphasize that the channel functions $\Phi_\mu(R;\Omega)$ exhibit an antinode at $\alpha = 45^\circ$ exactly or approximately. For $A = -1$, we emphasize that these channel functions exhibit a node at $\alpha = 45^\circ$ exactly or approximately. Channels that do not have either properties are assigned to have $A = 0$ and they are similar to singly excited states of two-electron atoms. This new classification scheme is valid for *all* states of two-electron atoms, i.e., it incorporates both singly and doubly excited states.

One important consequence of this new classification scheme is the observation that channels having identical $(K, T)^A$ but different $L, S,$ and π have isomorphic correlation patterns. This isomorphism results in nearly degenerate channel potential curves $U_\mu(R)$ as well as near-degeneracy of eigenenergies. This fact not only allows us to interpret the supermultiplet structure observed phenomenologically by Herrick and Kellman¹⁴ for intrashell states but also points out other new supermultiplets. In fact, we point out that *supermultiplet structure exists for all doubly excited states which have radial quantum number $A = +1$ or -1* . We also point out that supermultiplet structure does *not* exist for $A = 0$ states.

The rest of this paper is arranged as follows. In Sec. II we describe the labeling of potential curves $U_\mu(R)$ in

terms of correlation quantum numbers $K, T,$ and A and the rules for constructing correlation diagrams. In Sec. III we show the isomorphism of channels with identical $(K, T)^A$. This is illustrated by showing rotation-averaged surface charge densities for these channels. In Sec. IV we show how the isomorphism for $A = \pm 1$ channels results in supermultiplet structure. This is illustrated by grouping the energy levels calculated by Lipsky *et al.*¹¹ according to $(K, T)^A$. We emphasize that channels which have identical $(K, T)^\pm$ but with different L exhibit rotor-series structure in their energy eigenvalues. In the case that L is also identical but S and π are different, the eigenenergies are shown to exhibit near-degeneracy. We also consider how singly excited states fit into the present classification scheme and how are they related to $A = 0$ doubly excited states. In Sec. V, we summarize by recommending new symbols for labeling doubly excited states. In Appendix A the formulas for calculating rotation-averaged surface charge densities are given. In Appendix B, the classifications of Lipsky *et al.* for all doubly excited states of He below $N = 2$ and 3 and $L \leq 3$ are compared with the present $(K, T)^A$ classification. All the examples considered in this paper are for doubly excited states of He below $N = 3$ unless otherwise stated. Other examples will be considered in the future.

II. POTENTIAL CURVES AND CORRELATION RULES

A. Diabatic potential curves

We assume wave functions of doubly excited states are quasiseparable in hyperspherical coordinates³ and that they can be approximated as $F_\mu^n(R)\Phi_\mu(R;\Omega)$. The channel functions $\Phi_\mu(R;\Omega)$ and the channel potentials $U_\mu(R)$ are obtained by solving the two-electron Schrödinger equation in hyperspherical coordinates with R treated parametrically. The method used in calculating the channel functions $\Phi_\mu(R;\Omega)$ and channel potential curves $U_\mu(R)$ is similar to the method used in our previous works.⁵ Basically, analytical channel functions¹⁵ and hyperspherical harmonics are used to diagonalize the Schrödinger equation at each R in the adiabatic approximation. In order to preserve the correlation pattern for each channel, diabatic states are preferred in regions of avoided crossings. These diabatic curves are obtained presently by smoothly joining pairs of adiabatic potential curves at regions of avoid crossings. They can also be obtained more rigorously from adiabatic curves by introducing a 2×2 rotation matrix for each of the pair of curves involved.¹⁶ This last step is not done here but it is necessary for more accurate numerical calculations.

B. Potential curves converging to $\text{He}^+(N = 3)$ limits

We will use helium doubly excited states for discussion. Reduced units with $Z = 1$ are used throughout. In Fig. 1 diabatic potential curves for $1,3S^e, 1,3P^o,$ and $1,3D^e$ channels that converge to the $\text{He}^+(N = 3)$ thresholds are shown. Similar curves for $1,3F^o, 1,3G^e,$ and $1,3H^o$ are

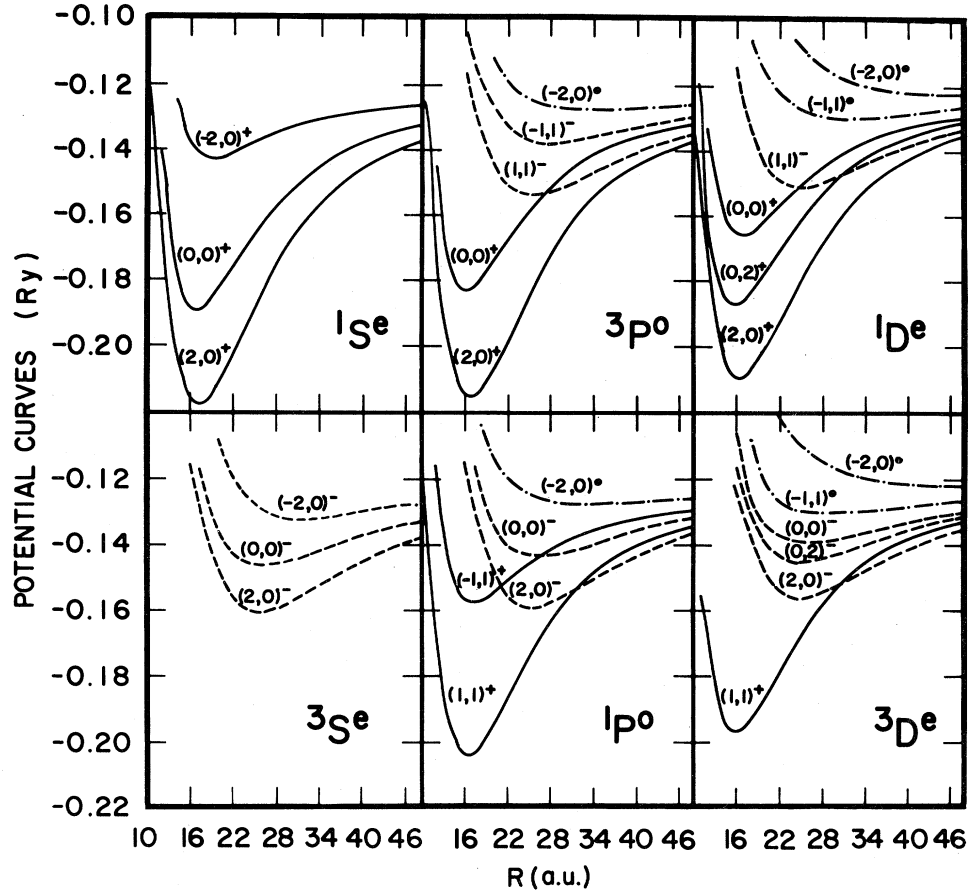


FIG. 1. Potential curves for all $1,3S^e$, $1,3P^o$, and $1,3D^e$ channels for He that converge to $\text{He}^+(N=3)$. Curves are labeled in terms of correlation quantum numbers as described in the text. Reduced units with $Z=1$ are used.

shown in Fig. 2. Two integer quantum numbers, K and T , in conjunction with one superscript, A , are used to designate each curve. The $+$ curves, corresponding to $A=+1$, are given in solid lines, while the $-$ curves, corresponding to $A=-1$, are given in dashed lines. For the $A=0$ curves, they are given in dashed-dotted lines. Only states with $\pi=(-1)^L$ are to be discussed below. States with $\pi=(-1)^{L+1}$ will be discussed in Sec. IV C.

From these potential curves we notice the following important features.

(1) All $1S^e$ channels belong to $A=+1$, all $3S^e$ channels belong to $A=-1$ and all $L \geq 5$ channels have $A=0$ only. For $1 \leq L \leq 4$, all three values of A , ± 1 and 0 , are allowed. Notice that the minimum of the potential curve for each $+$ channel occurs at $R \sim 16$, irrespective of the values of L , S , and π . For the $-$ channels the potential curves are in general shallower and the minimum for each curve occurs at $R \sim 24$. For channels with $A=0$ there are no pronounced potential wells and they are always the least attractive ones within the family of curves for a given L , S , and π .

(2) The $+$ curves have smaller centrifugal potentials at small R , thus states belonging to $+$ channels are more likely to penetrate into the small- R region. Penetration to

small- R region by states belonging to $-$ and 0 channels is less probable because of the larger centrifugal potential at small R .

(3) There is *no* definite ordering between $+$ and $-$ curves at large R , but all the $A=0$ curves correspond to the higher curves in the asymptotic limit. In the large- R region, potential curves corresponding to large K are lower. For a given K , larger T has lower potential.

(4) The noncrossing rule: Within the manifold of curves converging to a given $\text{He}^+(N)$ limit, only $+$ and $-$ curves can cross (sometimes more than once). Curves belonging to the same $+$, $-$, or 0 classifications do not cross, nor do $-$ and 0 curves cross.

C. The asymptotic limit: K and T quantum numbers for angular correlations

The observations above are followed by the curves shown in Figs. 1 and 2. Before studying the meaning of the superscript A we first examine the meaning of quantum numbers K and T . These two quantum numbers were first used by Herrick and Sinanoglu⁷ in their DESB functions for the classification of doubly excited states. The DESB functions are expressed as

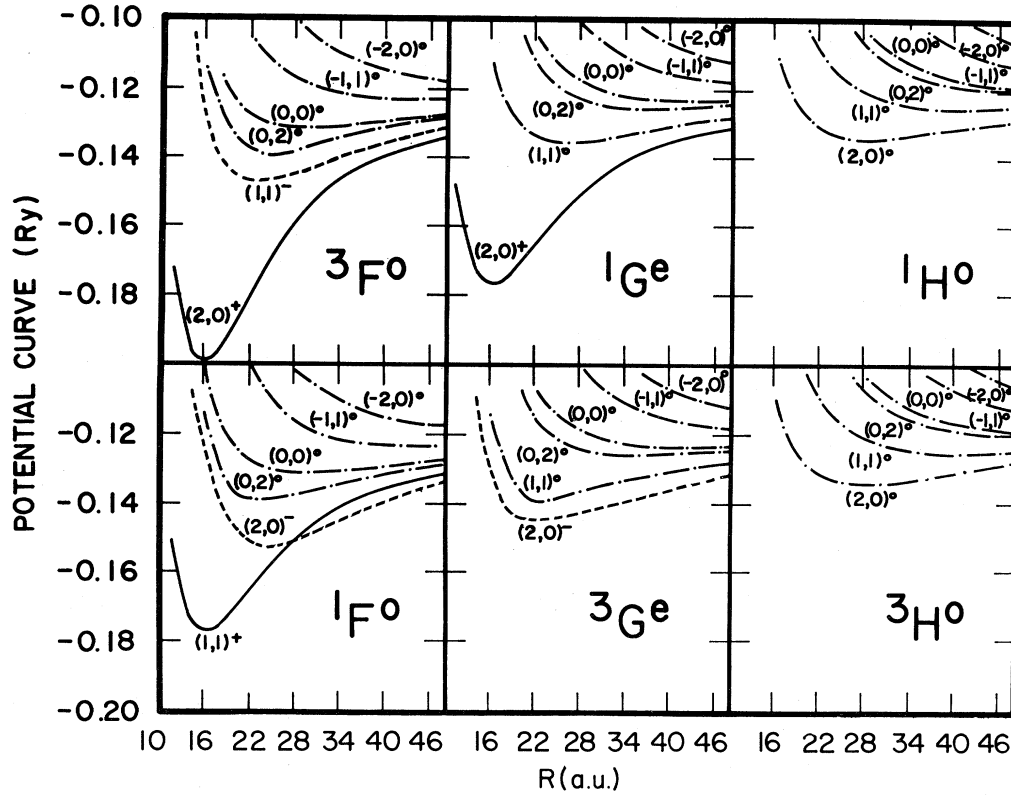


FIG. 2. Same as in Fig. 1 except for $1,3F^o$, $1,3G^e$, and $1,3H^o$ channels.

$$|Nn, KTLS\pi\rangle = \sum_{l,l'} |Nl, nl', LS\pi\rangle D_{Nl, nl'}^{KTL\pi}, \quad (1)$$

where D is proportional to a $9-j$ symbol and $|Nl, nl', LS\pi\rangle$ is a coupled two-electron hydrogenic wave function. Thus in (1), DESB functions are constructed as the linear combination of the product of hydrogenic wave functions for a given N and n . It is shown in Ref. 6 that DESB functions incorporate most of the angular correlations but not enough radial correlations. It is obvious that screening is not included in the expansion in (1).

Although the DESB functions are not adequate in representing doubly excited states, the integer quantum numbers K and T are convenient indices for labeling angular correlations. In fact, these two quantum numbers had also been used to label asymptotic dipole states¹³ for scattering systems like $e\text{-H}$, $e\text{-He}^+$, $e\text{-Li}^{2+}$, etc., i.e., they label Stark states which have long-range dipole interaction. In the asymptotic region, the dipole part of the potential is

$$V_d = \alpha_d / R^2. \quad (2)$$

Although there is no simple functional form relating α_d to K and T for a given N , L , S , and π , Herrick¹³ has shown that α_d , in reduced units, is given approximately by

$$\begin{aligned} \alpha_d = & -3N\lambda K + L(L+1) + \frac{1}{2}(N^2 - 1 - K^2 - 3T^2) \\ & - (K/12N\lambda)[8L(L+1) + N^2 - 1 - K^2 - 15T^2] \\ & + O(\lambda^{-2}), \end{aligned} \quad (3)$$

where $\lambda = 1/Z$. This formula is valid if λ is not too small and N not too large. Thus the asymptotic potential curves are ordered from below with decreasing values of K (i.e., maximum K corresponds to the lowest curve) and for a given K , with decreasing values of T . The curves shown in Figs. 1 and 2 follow this ordering in the asymptotic region.

For a given L and N , the range of K and T are determined as follows:⁷

$$T = 0, 1, \dots, \min(L, N-1), \quad (4a)$$

$$\pm K = N - T - 1, N - T - 3, \dots, 1 \text{ (or } 0). \quad (4b)$$

For states where $\pi = (-1)^{L+1}$, $T=0$ is not allowed. From Eqs. (4), we notice that the range of values for K and T for a given L and N is independent of S and π . For example, according to (4), the allowed values of (K, T) for $N=3$ are as follows: $(2, 0)$, $(0, 0)$, and $(-2, 0)$ for $1,3S^e$; $(2, 0)$, $(1, 1)$, $(0, 0)$, $(-1, 1)$, and $(-2, 0)$ for $1,3P^o$; and $(2, 0)$, $(1, 1)$, $(0, 2)$, $(0, 0)$, $(-1, 1)$, and $(-2, 0)$ for $L \geq 2$. For $\pi = (-1)^{L+1}$, the (K, T) pairs with $T=0$ are not allowed. Thus for $T \neq 0$, the allowed (K, T) pairs are independent of π .

The asymptotic dipole potential α_d , according to the perturbation formula (3), is independent of the overall parity π of the state for a given N , K , and T . In fact, this degeneracy has been proved by Nikitin and Ostrovsky^{13(b)} to be rigorously true based upon a group-theoretical explanation. Since for $T \neq 0$ the allowed (K, T) pairs for a given N and L are identical, we thus expect that the dipole po-

tentials are also identical.

In terms of the asymptotic properties of the two electrons, K is proportional to the average value of $r_1 \cos \theta_{12}$ where r_1 refers to the inner electron and θ_{12} has the usual meaning, and T^2 is proportional to the square of the average of $\vec{L} \cdot \hat{r}_2 = \vec{I}_1 \cdot \hat{r}_2$ (since $\vec{I}_2 \cdot \hat{r}_2 = 0$), thus T describes the magnitude of the overlap $\vec{I}_1 \cdot \hat{r}_2$, or roughly speaking, the relative orientation between the orbitals of the two electrons. If the two electrons orbits are on the same plane, then $T=0$.

D. The inner region: radial correlation quantum number A

The K and T quantum numbers discussed above in the asymptotic region can be continued into the small- R region since the angular correlation pattern has been shown^{5(d)} to be independent of R . To account for radial correlations at finite R , a value of $A = +1, -1$, or 0 is assigned to each (K, T) . Here *all* the $^1S^e$ curves have $A = +1$ and *all* $^3S^e$ curves have $A = -1$. This is because all $^1S^e$ channels have antinode at $\alpha = 45^\circ$ while all $^3S^e$ channels have node at $\alpha = 45^\circ$. In Figs. 1 and 2, all curves which have minima occurring at $R \sim 16$ are assigned to have $A = +1$, and those which have shallow minima at $R \sim 24$ are assigned to have $A = -1$. Such assignment implies (see Sec. III) that the channel functions for these curves have nearly antinodal (for $+$) or nodal (for $-$) characters at $\alpha \sim 45^\circ$. There are also high-lying curves in Figs. 1 and 2 which we have assigned $A = 0$. We will show in Sec. IVE that they are similar to singly excited states.

We have to know how to enumerate the number of possible $+$ and $-$ curves for a given N, L, S , and π . The number of $+$ curves is equal to the possible K and T pairs in Eq. (1) for $n=N$, which in turn is equal to the number of possible l and l' pairs (without violating the Pauli exclusion principle) for a given $n=N$. In other words, the number of $+$ curves is identical to the number of intrashell states for a given L, S , and π . Thus for $^{1,3}P^o$, the possible intrashell independent-particle states are $3s3p$ and $3p3d$. Thus there are two $+$ curves. For $^1D^e$, there are three $+$ curves by counting $3s3d, 3p^2$, and $3d^2$. For $^3D^e$, there is only one $+$ curve from $3s3d$ $^3D^e$. Because of the exchange symmetry, $+$ curves for $S=1$ become $-$ curves for $S=0$ and vice versa. Therefore, the number of $-$ curves for a given N, L, S , and π is obtained by counting the number of $+$ curves of the *other* spin symmetry. Thus, for example, there is one $-$ curve for $^1D^e$ and three $-$ curves for $^3D^e$. Curves which are not $+$ nor $-$ are assigned to $A=0$ and the number of $A=0$ channels is independent of S .

To complete the correlation rule for connecting the potential curves, it is necessary to assign (K, T) quantum numbers in the inner- R region. For the $+$ curves, the allowed K values have to satisfy the relation⁷

$$l + l' + K + S + N = \text{odd} \quad (5)$$

This condition originates from the symmetry requirement of the wave function at $r_1=r_2$. In Eq. (5), $l+l'$ enters only to indicate the parity of the channel. Thus the al-

lowed largest value of K for $^1P^o$ is $K=1$ and for $^3P^o$ is $K=2$ (for $N=3$). Since, from (5), K is either even or odd for all $+$ channels, the next allowed value of K for $^1P^o$ is $K=-1$ and for $^3P^o$ is $K=0$. Thus the $+$ curves for $^1P^o$ are $(1,1)^+$ and $(-1,1)^+$ and for $^3P^o$ are $(2,0)^+$ and $(0,0)^+$. To find (K, T) for the $-$ curves, recall that we have to refer to the $+$ channels of the *other* spin symmetry. Thus the $-$ channels for $^1P^o$ are $(2,0)^-$ and $(0,0)^-$ and for $^3P^o$ are $(1,1)^-$ and $(-1,1)^-$. If there is more than one value of T for a given K , then all the (K, T) pairs are assigned to have identical $+$ or $-$ characters. Thus for $^1D^e$ the $+$ channels are $(2,0)^+, (0,2)^+$, and $(0,0)^+$ and the $-$ channel is $(1,1)^-$. For $^3D^e$, the $+$ channel is $(1,1)^+$, the $-$ channels are $(2,0)^-, (0,2)^-$, and $(0,0)^-$. For other L, S , and π , the $+$ and $-$ channels are shown in Figs. 1 and 2. Notice that there are no $+$ and $-$ channels for $L > 4$ or for $L > 2(N-1)$ in general.

For a given A , the potential curves at small R are ordered from below with decreasing K and for a given K , with decreasing T . The $+$ curves have deeper potential wells with minima at smaller R and the $-$ curves have shallow potential wells with minima at larger R . On the other hand, in the asymptotic region, only the values of K and T count. By joining curves with identical (K, T) in the two regions, the $+$ and $-$ curves, in general, will cross, while the curves within a given A do not cross with each other. We also do not allow $-$ and 0 curves to cross since the 0 curves always correspond to smaller K .

E. The correlation rule

We summarize the resulting correlation rules.

(1) For a given N, L, S , and π , find the possible pairs of (K, T) from Eq. (4). The asymptotic potential curves are ordered from the bottom starting with the maximum allowable K and then in the order of decreasing K . If there is more than one value of T for a given K , order from below according to decreasing value of T .

(2) Compute the number of $+$ curves for a given N, L, S , and π by enumerating the number of independent-electron states consisting of identical principal quantum numbers. Find the K values for $+$ curves which satisfy Eq. (5). They are either all even or all odd integers. By starting with the largest K allowed, label all the $+$ curves in the small- R region from below with decreasing values of K and for a given K , with decreasing values of T , until all the $+$ curves are accounted for. Find the number of $-$ curves by computing the number of $+$ curves of the other spin symmetry. Connect curves with identical (K, T) from the inner to the outer region. Only $+$ and $-$ curves are allowed to cross and all the rest follow the non-crossing rule.

III. RADIAL AND ANGULAR CORRELATIONS

A. Summary of correlations for $^1S^e$ and $^3S^e$ channels

In this section we show that the set of quantum numbers K, T , and A implies distinct radial and angular correlations. In our previous works⁵ for $L=0$ states, this is achieved by displaying the surface charge densities $|\Phi_\mu(R; \Omega)|^2$ on the (α, θ_{12}) plane. From these works, we

conclude that (1) the surface charge-density profiles evolve smoothly with R such that channel characters are preserved; (2) angular correlation for a given channel does not vary significantly, while radial correlation evolves smoothly such that charge densities near $\alpha=45^\circ$ shift gradually away from $\alpha=45^\circ$ as R increases; and (3) angular correlation pattern is essentially independent of $S=0$ or $S=1$ for corresponding channels (channels with identical K and T), the difference is being in the α distribution near $\alpha=45^\circ$ where $^1S^e$ channels have an antinode and $^3S^e$ channels have a node at $\alpha=45^\circ$.

B. Correlations for $L \neq 0$ channels

Channel wave functions $\Phi_\mu(R; \Omega)$ for $L \neq 0$ states depend not only on the internal angles α and θ_{12} but also on three external angles, e.g., the three Euler angles. Unlike classical systems, exchange symmetry precludes the wave functions from being expressed as the product of functions of internal and external coordinates. To exhibit the internal correlation structure, we calculate the rotation-averaged surface charge densities^{8,16-18}

$$\begin{aligned} \sigma_\mu(R; \alpha, \theta_{12}) &= \langle \Phi_\mu(R; \Omega') | \delta(\alpha' - \alpha) \\ &\quad \times \delta(\cos\theta'_{12} - \cos\theta_{12}) | \Phi_\mu(R; \Omega') \rangle. \end{aligned} \quad (6)$$

The explicit expression of $\sigma_\mu(R; \alpha, \theta_{12})$ is given in Appendix A. This definition of σ_μ reduces to the one used earlier for $L=0$ states.

C. Isomorphism of channels with identical $(K, T)^A$

All doubly excited states that have identical $(K, T)^A$ quantum numbers are isomorphic, i.e., they have similar correlation patterns. To illustrate this isomorphism, we show in Fig. 3 the surface charge-density plots of the $(2,0)^+$ channel of $^1S^e$, $^3P^o$, $^1D^e$, and $^3F^o$ at $R=20$ for $N=3$. Both surface plots and contour plots are shown together in order to illustrate the overall picture as well as the greater quantitative details. For the contour plots, α is shown only between 0 and $\pi/4$ due to the apparent symmetry of surface charge densities with respect to $\alpha=\pi/4$. From the surface plots, it is obvious that all four plots appear quite similar. The charge densities have a pronounced peak at $\alpha=\pi/4$ and $\theta_{12}=\pi$ with little concentration for $\theta_{12} < \pi/2$. This type of charge distribution resembles that of a linear XYX molecule where X refers to the electron and Y to the nucleus. This analogy of course is rather limited since deviation of charge distribution from the "equilibrium" point $\alpha=\pi/4$ and $\theta_{12}=\pi$ is not very small. We also notice that in each case there is a secondary peak near $\alpha \sim 0$ (and $\alpha \sim \pi/2$). While this secondary peak is more pronounced near $\theta_{12} \sim \pi$ for $^1S^e$, it becomes more pronounced near $\theta_{12} \sim 0$ for $^3F^o$. Examination of the contour plots also shows that the central peak around $\alpha=\pi/4$ and $\theta_{12}=\pi$ is broader for $^3F^o$ and narrower for $^1S^e$. This is an indication of the centrifugal distortion of correlation patterns for higher L channels. In Fig. 4 the surface charge densities along θ_{12} for $\alpha=45^\circ$ and along α

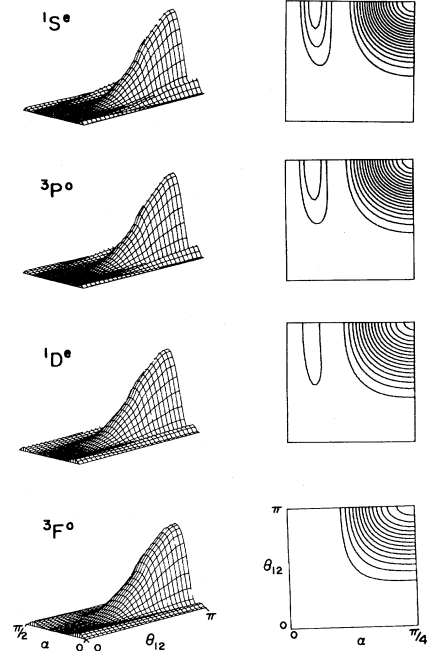


FIG. 3. Surface charge densities for the $(2,0)^+$ channel of $^1S^e$, $^3P^o$, $^1D^e$, and $^3F^o$ of He at $R=20$. Contour plots indicate that the distribution near the peak at $\alpha=45^\circ$ and $\theta_{12}=\pi$ is sharper for $^1S^e$ and becomes broader for higher L .

for $\theta_{12}=\pi$ are displayed. The θ_{12} dependence displayed here is similar to that obtained by Ezra and Berry⁸ where angular correlation in a model atom between two electrons on a spherical surface was studied.

Isomorphism is a general property for channels with

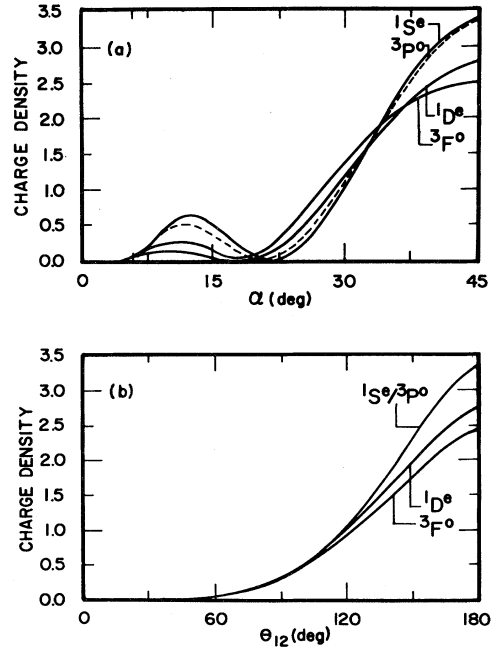


FIG. 4. Surface charge densities (a) vs α at $\theta_{12}=\pi$ and (b) vs θ_{12} at $\alpha=45^\circ$ for the $(2,0)^+$ channels of $^1S^e$, $^3P^o$, $^1D^e$, and $^3F^o$ of He at $R=20$. For (b), the charge densities along θ_{12} for $^1S^e$ and $^3P^o$ cannot be distinguished within the scale shown.

identical $(K, T)^A$. In Fig. 5 we show two more examples of such isomorphism for the $(1, 1)^+$ channels of ${}^1P^o$ and ${}^3D^e$ at $R=20$ and the $(1, 1)^-$ channels of ${}^3P^o$ at $R=27$ and ${}^1D^e$ at $R=32$ for $N=3$ (these graphs are shown at different values of R to avoid the region of curve crossing). We also notice that the major difference between the $(1, 1)^+$ ${}^1P^o$ channel and the $(1, 1)^-$ ${}^3P^o$ channel is in radial correlations where the $+$ channel has large charge concentration near $\alpha \sim 45^\circ$ while the $-$ channel has near-zero charge concentration for $\alpha \sim 45^\circ$ for all values of R . This is also true for the $(1, 1)^+$ ${}^3D^e$ channel, as well as for other channels which have identical (K, T) .

D. Correlations and $(K, T)^A$

We have shown that angular correlation patterns are basically independent of A for a given (K, T) [cf. the $(1, 1)^+$ and $(1, 1)^-$ channels shown in Fig. 5] but differ significantly for channels with different (K, T) . In the discussion to follow, it is assumed that the invariance of angular correlation and the evolution of radial correlation from the inner- to outer- R regions are already understood. To minimize the number of graphs to be displayed, we show σ_μ for different $(K, T)^A$ channels at large R where σ_μ at $\alpha \sim 45^\circ$ is nearly vanishing. In this limit, the charge densities are independent of $S=0$ or 1.

In Fig. 6 the surface charge densities σ_μ for all the ${}^1S^e$, ${}^1P^o$, and ${}^1D^e$ channels for $N=3$ are displayed at the asymptotic $R=36$. They are ordered such that every graph across each row has identical (K, T) , although the values for A are sometimes different. We notice the isomorphic angular correlations across each row.

Figure 6 also illustrates the dependence of angular correlation on quantum number K . For a given T , large K values correspond to the situation that the two electrons are distributed with large θ_{12} and negative K values correspond to small θ_{12} ($< \pi/2$). Recall that K is proportional to $\langle \cos\theta_{12} \rangle$; it offers no information about the θ_{12} distri-

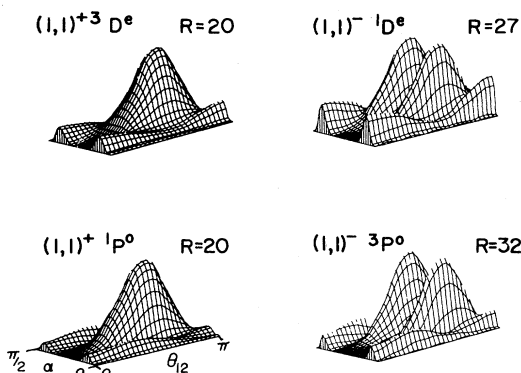


FIG. 5. Surface charge densities for the $(1, 1)^+$ ${}^3D^e$ and $(1, 1)^+$ ${}^1P^o$ channels at $R=20$, the $(1, 1)^-$ ${}^1D^e$ channel at $R=27$ and the $(1, 1)^-$ ${}^3P^o$ channel at $R=32$. Notice that the pairs of $(1, 1)^+$ and of $(1, 1)^-$ channels have similar correlation patterns. The major difference between $(1, 1)^+$ and $(1, 1)^-$ channels is near the $\alpha=45^\circ$ line. Notice that the angular distribution (in θ_{12}) does not differ significantly for the $(1, 1)^+$ and $(1, 1)^-$ channels.

bution itself. Thus the $(0, 2)$ and $(0, 0)$ channels in Fig. 6, although having nearly identical $\langle \cos\theta_{12} \rangle \sim 0$, their actual σ_μ 's are quite different for the two channels. In Fig. 6, it appears that the σ_μ for the $(0, 2)$ ${}^1D^e$ channel is quite close to that for the $(1, 1)$ ${}^1D^e$ channel. This is actually not so. It is due to the fact that the plots are in the "asymptotic" region. In Fig. 7, the surface charge-density plots for $(0, 2)^+$ and $(1, 1)^-$ channels of ${}^1D^e$ are shown at $R=20$ where the $+$ and $-$ characters of the $(0, 2)^+$ and $(1, 1)^-$ channels are clearly observed.

IV. SPECTROSCOPY AND SUPERMULTIPLY STRUCTURE

A. Potential curves grouped according to $(K, T)^A$

Examination of potential curves shown in Figs. 1 and 2 reveals that channels with identical $(K, T)^A$ have similar shapes and nearly identical values. In Fig. 8 we show groups of curves which have identical $(K, T)^A$. For a given $(K, T)^A$, we notice that curves belonging to higher L lie slightly higher.

The difference in potential curves for a given $(K, T)^A$ but different L can be interpreted as similar to the rotational distortion of potential curves of a "rigid" rotor. Energy eigenvalues calculated from these curves form an approximate rotor series. For example, the lowest eigenvalues from each of the $(2, 0)^+$ ${}^1S^e$, ${}^3P^o$, and ${}^1D^e$ curves in Fig. 8(a) can be fitted into a rotor series. Since the minima of all three curves occur at approximately the same R

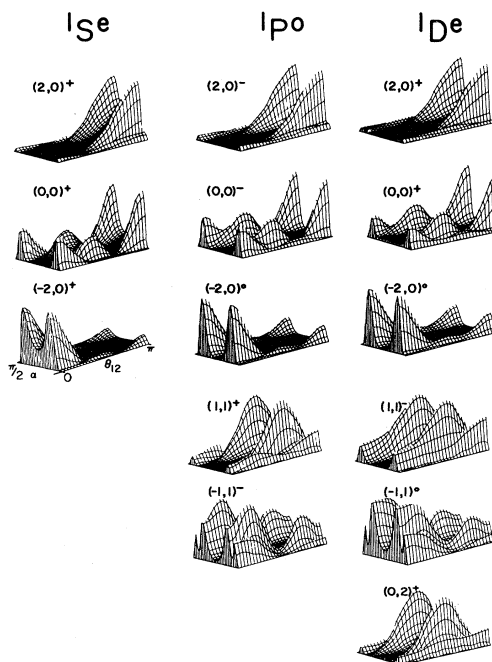


FIG. 6. Surface charge densities for all ${}^1S^e$, ${}^1P^o$, and ${}^1D^e$ channels below $N=3$ at $R=36$. In this asymptotic region, all charge densities near $\alpha=45^\circ$ become very small, thus only angular correlations are seen. These plots show that angular correlation is independent of radial correlation quantum number A .

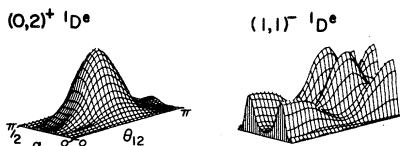


FIG. 7. Comparison of the surface charge densities for the $(0,2)^+ 1D^e$ and $(1,1)^- 1D^e$ channels at $R = 20$.

and all three curves have similar shapes, a single empirical moment of inertia can fit the spectra quite well.

If we calculate the lowest eigenvalues of each of the curves in Fig. 8(a), the resulting eigenvalues form a rotation-vibrational supermultiplet structure. This supermultiplet structure was first derived phenomenologically by Herrick and co-workers¹⁴ and applied only to intrashell states. In this paper we attribute this supermultiplet structure to systematic patterns of electron correlations as well as to the regular variation of potential curves, as shown in Figs. 8(a) and 8(b). This supermultiplet structure is *not* limited to intrashell states only. They are expected to exist for intershell states as well if $A = +1$ or -1 . On the other hand, such structure does not exist for states with $A = 0$. This is clear from the potential curves shown in Fig. 8(c) for the $(0,2)^0$ channels of $1,3F^o$, $1,3G^e$, and $1,3H^o$. The triplet curves are shown in dashed lines and are lower than the corresponding singlet curves shown in solid lines. The energy eigenvalues calculated from these curves are similar to the spectral pattern of singly excited states, i.e., energy values are quite different for different L and for a given L , triplets are slightly lower in energy than singlets (see Sec. IV E below).

B. Spectroscopy of helium below $N = 3$

In Fig. 9 energy levels for the low-lying states of He below $N = 3$ are grouped in terms of effective quantum numbers n^* using the data calculated by Lipsky *et al.*

Only states with $\pi = (-1)^L$ and states which have been identified with $A = +1$ and -1 are displayed. Along the horizontal axis, we show the correlation quantum numbers $(K, T)^A$. The similarity to a rotor series for each given $(K, T)^A$ is quite obvious, particularly for the lowest members of each $(K, T)^A$ group. For higher members, the rotor structure is not as good because the energies of these states are determined to a great extent by the different asymptotic potentials. On the other hand, it is quite evident that the rotor structure is not limited to intrashell states only. In Appendix B the correspondences between the $(K, T)^A$ channel classifications and those given by Lipsky *et al.* are compared.

According to the ordering in Fig. 9, we notice *two new regularities* of the spectroscopy of doubly excited states.

(1) According to the $(K, T)^A$ ordering, the rotor structure can be used to help determine the relative energy levels of various L , S , and π states. The "string" of each rotor series is determined by the possible number of L , S , and π states which have the required $(K, T)^A$. Notice that there are situations where the number of states in a rotor series is very small. For example, in Fig. 9 there is only one member for each of the $(0,2)^\pm$, $(-1,1)^\pm$, and $(-2,0)^\pm$ series.

(2) There is a "repetition" of $(K, T)^+$ and $(K, T)^-$ rotor structure. Recall that for a given (K, T) , if $A = +1$ for $S = 0$, then $A = -1$ for $S = 1$ and vice versa. Thus the rotor series for $(K, T)^-$ can be obtained from the rotor series for $(K, T)^+$ simply by interchanging the spins. For example, the $1S^e-3P^o-1D^e-3F^o-1G^e$ rotor series for $(2,0)^+$ is "repeated" as the $3S^e-1P^o-3D^e-1F^o-3G^e$ rotor series for $(2,0)^-$ ($3,1G^e$ levels are not included in Fig. 9 since they are not available from Ref. 11). We emphasize that the rotor series is evident for $A = \pm 1$ states only. For $A = 0$, no such structure is observed.

In constructing the energy-level diagram in Fig. 9, we found that the second $(0,0)^+ 1D^e$ state is not listed in Ref. 11. This level is shown in Fig. 9 in dashed lines. Its position was estimated using the assumption of constant quan-

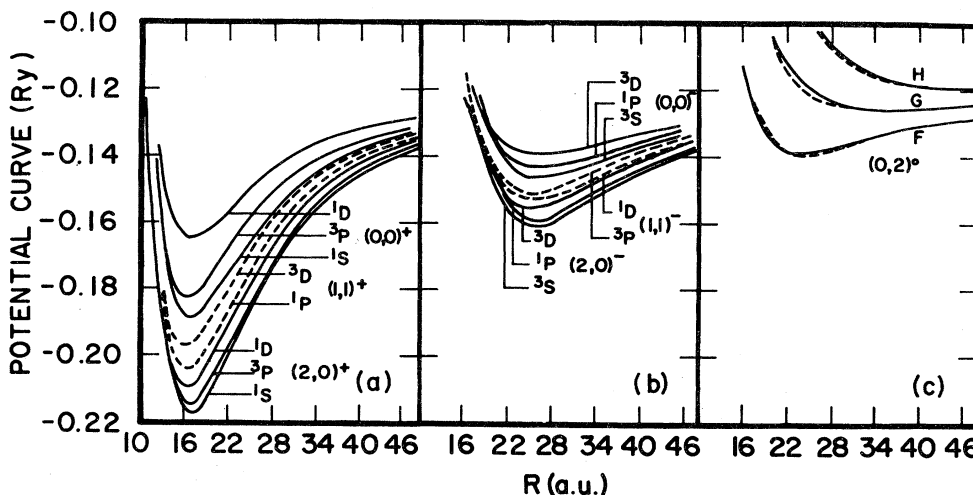


FIG. 8. Potential curves grouped according to $(K, T)^A$ quantum numbers. For a given $(K, T)^A$, higher L gives correspondingly higher potentials at large R .

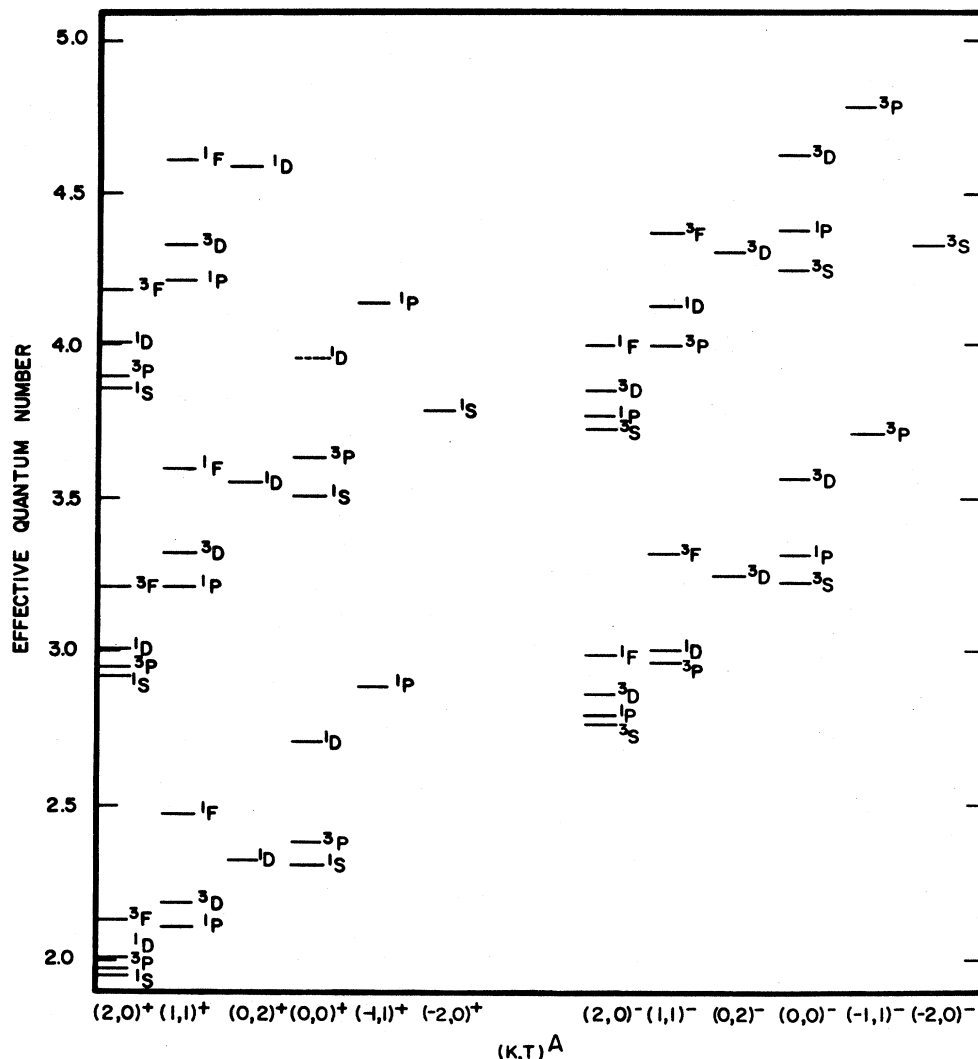


FIG. 9. Effective quantum numbers n^* grouped according to $(K, T)^+$ and $(K, T)^-$ quantum numbers. Parity of each state is $\pi = (-1)^L$. Notice the rotorlike structure for a given $(K, T)^+$ and $(K, T)^-$. These energy levels are taken from the calculation of Lipisky *et al.* (Ref. 11). A complete rotor series for $(2, 0)^+$ would include ${}^1G^e$ and for $(2, 0)^-$ would include ${}^3G^e$ except that these levels are not available from Ref. 11. See text for some modification of the classification from Ref. 11.

tum defect along the series.

The second and third members (as well as the higher members not shown) of the $(1, 1)^+ {}^1F^o$ channel shown in Fig. 9 are classified differently from those given in Ref. 11. The reason for this new assignment is given in Sec. IV C.

C. $\pi = (-1)^{L+1}$ states

All the channels considered so far have $\pi = (-1)^L$. For states where $\pi = (-1)^{L+1}$, $T = 0$ channels are not allowed. According to (4), the number of (K, T) pairs for $T \neq 0$ is independent of the overall parity for a given N and L . In addition, the quantum numbers K , T , and A for $\pi = (-1)^L$, $S = 0$ channels are identical to those for $\pi = (-1)^{L+1}$, $S = 1$ channels. Similarly, the K , T , and A quantum numbers for $\pi = (-1)^L$, $S = 1$ channels are identical to those for $\pi = (-1)^{L+1}$, $S = 0$ channels. For exam-

ple, the two ${}^3P^e$ channels (for $N = 3$) are $(1, 1)^+$ and $(-1, 1)^+$. These are the two $T \neq 0$ channels for ${}^1P^o$. Similarly, the three ${}^1D^o$ channels are $(1, 1)^+$, $(0, 2)^-$, and $(-1, 0)^0$. These are the three $T \neq 0$ channels for ${}^3D^e$. Therefore, we found pairs like ${}^3P^e$ - ${}^1P^o$, ${}^1P^e$ - ${}^3P^o$, ${}^3D^o$ - ${}^1D^e$, ${}^1D^o$ - ${}^3D^e$, etc., have identical $(K, T)^A$ channels if all the $T \neq 0$ channels are excluded.

These identical $(K, T)^A$ pairs also result in isomorphic correlations. In Fig. 10 the asymptotic correlation patterns at $R = 36$ are shown for ${}^1P^e$ and ${}^1D^o$ channels belonging to $N = 3$. Channels across each row have identical (K, T) and isomorphic correlations. These surface charge-density plots should be compared to similar plots in Fig. 6 for $T > 0$ channels. It is quite obvious that channels with identical $(K, T)^A$ are isomorphic. The major difference occurs at $\theta_{12} = 0$ and π where the charge densities for $\pi = (-1)^{L+1}$ channels vanish. Since the asymptotic potential does not depend on S and π [see Eq. (3)],

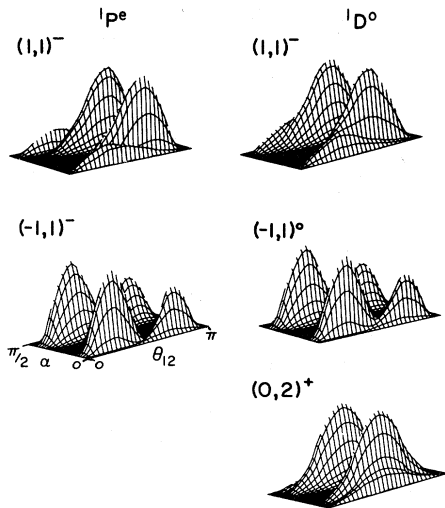


FIG. 10. "Asymptotic" correlation patterns for all the ${}^1P^e$ and ${}^1D^o$ channels below $N=3$ at $R=36$. These plots should be compared with plots of identical (K, T) shown in Fig. 6.

these isomorphic channels also have identical asymptotic potentials, thus we expect that the potential curves for identical $(K, T)^A$ channels remain almost degenerate throughout the whole range of R , despite the fact that the parities are different. Such near-degeneracy implies that

the energy levels for *all* states calculated from the corresponding channels will remain nearly degenerate. In Fig. 11 the effective quantum numbers n^* from the data of Lipsky *et al.* are compared for channels with identical $(K, T)^A$. States with $\pi=(-1)^L$ are shown in solid lines and states with $\pi=(-1)^{L+1}$ are shown in dashed lines. It is easily noticed that the energies are nearly independent of the overall parity if the correlation quantum numbers are identical.

In constructing Fig. 11, we have interchanged the classification given in Ref. 11 for the $(3,na)$ and $(3,nc)$ states of ${}^1F^o$ for $n \geq 4$. This new assignment results in more regular spectral behavior such that the near-degeneracy with ${}^3F^e$ states is maintained for both $(1,1)^+$ and $(0,2)^0$ channels.

Unlike the rotor-series structure, the near-degeneracy for states with identical $(K, T)^A$ and L (but different S) does not depend on the values of A . In Fig. 11 we show that the near-degeneracy is true for $A=0$ states also.

For channels with $\pi=(-1)^{L+1}$, there also exists a one-to-one mapping from the $N, K, T, L, \pi=(-1)^{L+1}$ channel to the $N-1, K-1, T-1, L-1, \pi=(-1)^L$ channel if the spin quantum numbers are also interchanged. In Fig. 12 the potential curves for ${}^{1,3}P^e, {}^{1,3}D^o$, and ${}^{1,3}F^e$ channels for $N=4$ are shown. Notice that there is a one-to-one correspondence between the number of channels and the shape of each potential curve, for example, between the ${}^1S^e$ curves in Fig. 1 and ${}^3P^e$ curves in Fig.

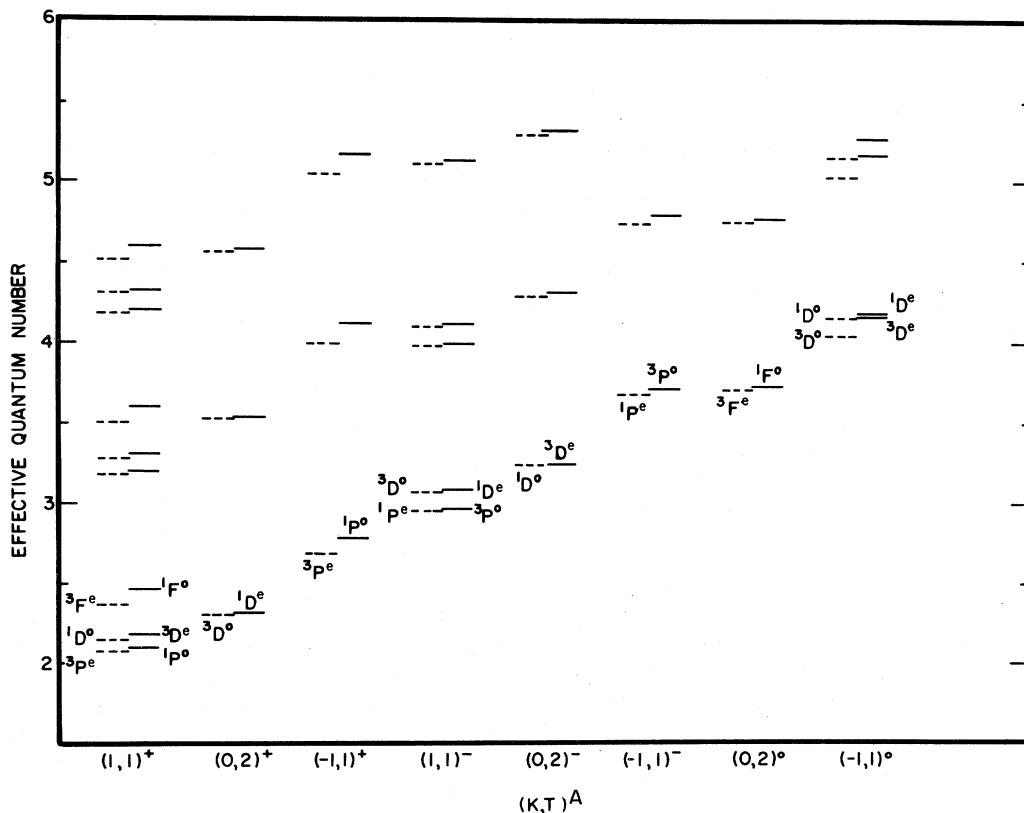


FIG. 11. Effective quantum numbers n^* grouped according to $(K, T)^A$ for $\pi=(-1)^L$ and $(-1)^{L+1}$ states. Only $T>0$ states are shown. Notice the near-degeneracy of states with identical L but different S and π . Higher members of each column are not labeled as they follow the pattern of the lower members. Data are from Ref. 11.

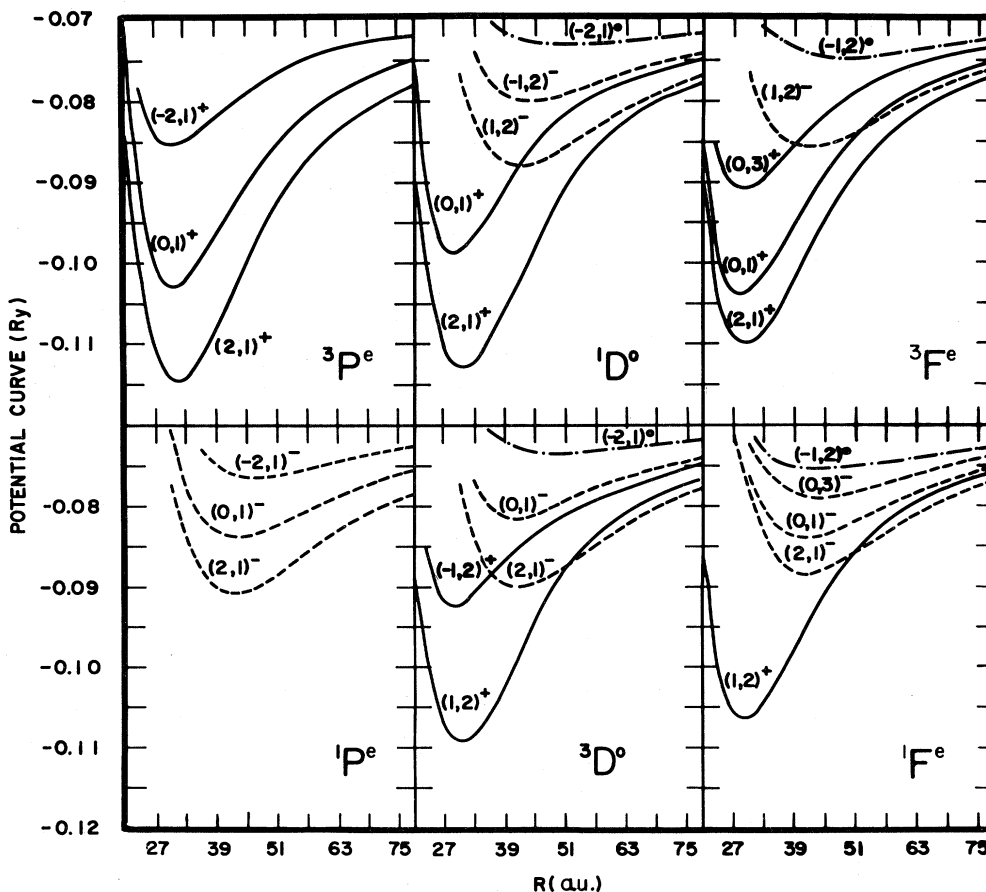


FIG. 12. Potential curves for all $1,3P^e$, $1,3D^o$, and $1,3F^e$ channels below $N=4$. These curves are to be compared with curves shown in Fig. 1.

12. Similar relations for other pairs, $3S^e-1P^e$, $1P^o-3D^o$, and $3P^o-1D^o$, are easily seen. However, it should be noted that this one-to-one mapping does not imply isomorphic correlations since their correlation quantum numbers are different.

D. Singly excited states

According to the present classification scheme, all the singly excited states have $(K,T)=(0,0)$. The channel quantum numbers are $(0,0)^+$ for $1S^e$, $(0,0)^-$ for $3S^e$, and $(0,0)^0$ for all other singly excited states. Within the independent-particle model the energy for $1snL^3L$ is always lower than the energy for $1snL^1L$ for all two-electron atoms. This is understood in terms of Pauli exchange correlations that the two electrons in triplet states are kept away from each other because of identical spin orientations, thus reducing the electron-electron repulsion. To understand that this results in different angular correlations, in Fig. 13 the surface charge-density plots for $1P^o$ and $3P^o$ singly excited states are shown at $R=2, 4$, and 6 . Notice that at $R=2$, angular correlation is such that the two electrons are to stay near $\theta_{12}=\pi$ for $3P^o$ and near $\theta_{12}=0$ for $1P^o$. At large R (≥ 4), we notice that the degree of angular correlation becomes less pronounced as the surface charge densities become independent of θ_{12} at large R .

E. Doubly excited states with $A=0$

Except for $1,3S^e$ and $1,3P^e$, all doubly excited states for other L, S , and π have states belonging to $A=0$. If $L > 2(N-1)$, then all the channels have $A=0$. The best known example of an $A=0$ channel is the so-called $2pnd^1P^o$ series [designated as $(-1,0)^0 1P^o$ here] of He. Such an independent-particle designation actually is not adequate. Configuration-interaction calculations have shown that these states have large configuration mixing with the $(0,1)^+$ series. It was shown in Ref. 6 that the channel function for $2pnd^1P^o$ series is characterized by vanishing charge densities near $\alpha \sim 45^\circ$ for all values of R . Such properties are readily reproduced in the present approach using quasiseparability of wave functions in hyperspherical coordinates.

For a given L, S, π , and N , if $A=+1$ and/or $A=-1$ channels exist, then $A=0$ channels are characterized by vanishing charge densities near $\alpha \sim 45^\circ$ and large charge concentrations at small θ_{12} . For $L > 2(N-1)$, there are no $+$ and $-$ channels and some $A=0$ channels can have charge densities near $\alpha \sim 45^\circ$ similar to those shown in Fig. 13 for singly excited states. The correlation patterns for these channels are not very sharp (or as strongly correlated). Different channels are basically distinguished by small differences in θ_{12} distribution.

Recall that for $A=0$ states there is no rotor-series

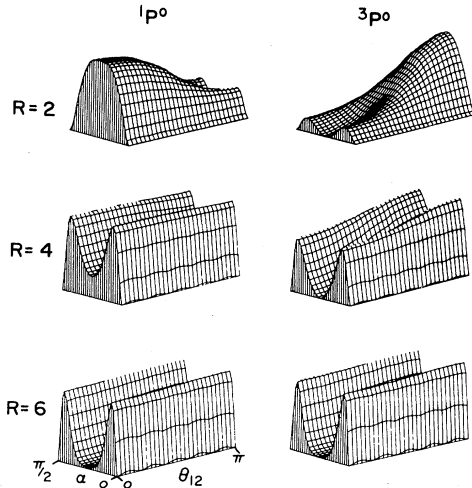


FIG. 13. Surface charge densities for $1snp\ ^1P^0$ and $1snp\ ^3P^0$ channels at $R=2, 4$, and 6 . Notice that Pauli exchange correlation is reflected as angular correlation in charge-density distributions.

structure. In fact, for a given n, N, K, T, L , and π , the triplet always lies below the singlet. In Fig. 14 we show the effective quantum number n^* for $A=0$ states calculated by Lipsky *et al.* In all the cases shown, singlet and triplet states are almost completely degenerate except for

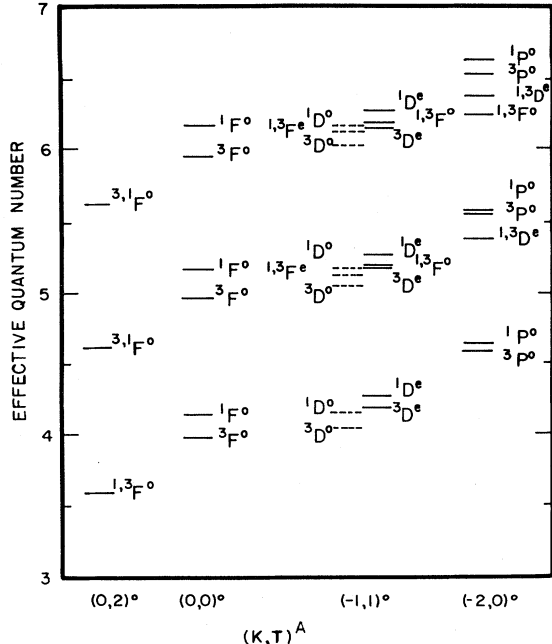


FIG. 14. Effective quantum numbers n^* for the $A=0$ channels grouped according to $(K, T)^0$. Notice that the triplet state is always below the singlet state for a given $(K, T)^0, L$, and π . For states that are nearly degenerate that cannot be distinguished in the diagram, for example, when $^1D^e$ is slightly above $^3D^e$, the levels are indicated as $^{1,3}D^e$ in the diagram. The two lines labeled $^{3,1}F^0$ indicate that $^3F^0$ is slightly above $^1F^0$, but this is likely the result of insufficient numerical accuracy in the calculation. Data are from Ref. 11.

one channel for each L . Thus, for $^1F^0$ and $^3F^0$, the singlet-triplet separation is relatively large for the $(0,0)^0$ channel; for all other channels the singlet and triplet are almost degenerate and cannot be distinguished in the graph. Thus we use $^{1,3}F^0$ to indicate that $^1F^0$ is slightly higher than $^3F^0$. For the $(0,2)^0$ channel, we have $^{3,1}F^0$ indicating that $^3F^0$ is higher than $^1F^0$. This could be the result of inaccuracy in the calculation. For $^{1,3}D^e$, the singlet-triplet separation is large for the $(-1,1)^0$ channel but quite small for the $(-2,0)^0$ channel.

V. DESIGNATION OF DOUBLY EXCITED STATES

The present analysis allows us to introduce new notations for designating doubly excited states. We recommend that each state be denoted by

$$|\phi\rangle \equiv |n(K, T)_N^A\ 2S+1L^\pi\rangle.$$

This notation is *unique* for each doubly excited state. It is to replace the inadequate notation, such as $n|N|'2S+1L^\pi$, which is based upon the independent-particle model. As noted in this paper, each quantum number in the present notation has well-defined physical meaning. The correlation quantum numbers K, T , and A describe the correlation pattern of the state, while N is the dissociation limit of the channel or the principal quantum number of the inner electron, and n is the principal quantum number of the outer electron. To describe a given channel or a Rydberg series, we use the notation

$$\mu \equiv |(K, T)_N^A\ 2S+1L^\pi\rangle.$$

According to the present recommended notation, the three $^1P^0$ channels below $N=2$ are $(0,1)_2^+{}^1P^0$, $(1,0)_2^-{}^1P^0$, and $(-1,0)_2^0{}^1P^0$. This is to replace the $2snp + 2pns\ ^1P^0$, $2snp - 2pns\ ^1P^0$, and $2pnd\ ^1P^0$ notations used by Cooper *et al.*² This latter designation emphasizes radial correlation only and cannot be generalized to other doubly excited states easily.

The present notation is also more general than the notation $|n, N, K, T, 2S+1L^\pi\rangle$ used in the DESB functions. The DESB designation alone does not provide information about radial correlation. Furthermore, the present notation does imply that each state has approximate wave function $F_\mu^n(R)\Phi_\mu(R; \Omega)$, and that there are well-defined procedures⁵ for calculating these functions. The validity of this representation and the failure of DESB functions have been examined in Refs. 5(c) and 6 separately.

To be consistent with the principal quantum numbers used in the independent-particle model as well as in the DESB functions, the smallest principal quantum number n of the outer electron is chosen as follows.

(i) The lowest n for all $A=+1$ channels is $n_{\min}=N$.

(ii) The lowest n for all $A=-1$ channels is $n_{\min}=N+1$.

(iii) The lowest n for the lowest $A=0$ channel is $n_{\min}=N+1$, successive higher $A=0$ channels have n_{\min} increase by one unit for each $\Delta K=-1$, successive channels with identical K but different T have the same n_{\min} .

Accordingly, the lowest states for each of the given $^1P^0$ channels below $N=3$ are ${}_3(1,1)_3^+$, ${}_4(2,0)_3^-$, ${}_3(-1,1)_3^+$,

$4(0,0)_3^-$, and $4(-2,0)_3^0$ $1P^o$. Similarly, for the six $1F^o$ channels below $N=3$, the lowest states are $3(1,1)_3^+$, $4(2,0)_3^-$, $4(0,2)_3^0$, $4(0,0)_3^0$, $5(-1,1)_3^0$, and $6(-2,0)_3^0$ $1F^o$. These rules also work for high angular momentum states where every state belongs to $A=0$. For example, the six channels for $1,3H^o$ have the following lowest states: $4(2,0)_3^0$, $5(1,1)_3^0$, $6(0,2)_3^0$, $6(0,0)_3^0$, $7(-1,1)_3^0$, and $8(-2,0)_3^0$ $1,3H^o$. Recall that the lowest single-particle states are $3s6h$, $3p5g$, $3p7i$, $3d4f$, $3d6h$, and $3d8k$ for $1,3H^o$. Therefore, the lowest n 's are 4, 5, 6, 6, 7, and 8, as predicted by the rules.

Since the lowest state for each channel does not have nodes in the radial function $F_\mu^n(R)$, the number of radial nodes for each state is $n - n_{\min}$ where n_{\min} is the lowest principal quantum number of that channel. Although the size of the state, as measured by the radial distribution of $F_\mu^n(R)$, is reasonably represented by the quantum number n , the energy of the state is not. This is due to the large variation of quantum defects for different channels, as the simultaneous penetration of the two electrons into the small- R region is quite different for different channels.

VI. DISCUSSION

In this paper we have introduced a complete classification scheme for doubly excited states of two-electron atoms. Three quantum numbers K , T , and A are used to describe correlations. The integer K and T quantum numbers, adopted from the group-theoretical work of Herrick and Sinanoglu, were used to describe angular correlations. The radial correlation quantum number A is assigned to take $+1$, -1 , and 0 only. In terms of $(K, T)^A$, the correlation pattern is identified. It has been shown that states with identical $(K, T)^A$ but different L , S , and π exhibit similar correlation patterns. Such isomorphism is shown to result in general supermultiplet structure for doubly excited states.

In terms of these quantum numbers, each doubly excited state, designated as $|n(K, T)_N^A 2S+1L^\pi\rangle$, to first order, is expressed in hyperspherical coordinates as $F_\mu^n(R)\Phi_\mu(R; \Omega)$. Here n corresponds to the principal quantum number of the outer electron and the channel index $\mu \equiv |(K, T)_N^A 2S+1L^\pi\rangle$, where N is the dissociation limit of the channel, K , T , and A describe internal correlations, and L , S , and π are the usual quantum numbers for the system as a whole. From the examples discussed in this paper, it is easy to visualize the correlation pattern for each set of $(K, T)^A$. Therefore, the assigned quantum numbers are not only unique for each state, but also provide important information about electron correlations. In other words, our new designation provides the needed terminology for describing doubly excited states. They are equivalent to the independent-particle model for describing singly excited states.

This classification scheme also identifies several new spectroscopic regularities, as shown in Figs. 9 and 11. By grouping energy levels according to $(K, T)^A$, one can easily locate the missing lines and possible misidentifications. We have pointed out two examples in this paper already.

The current classification scheme also indicates approximate selection rules for electron-atom and photon-atom

collisions. For example, photoabsorption of helium from ground state to the neighborhood of $\text{He}^+(N=3)$, in principle, should give five $1P^o$ series. The experiment by Woodruff and Samson¹⁹ has shown that only one predominant $(1,1)_3^+$ channel was observed near $N=3$, with slight evidence of the $(-1,1)_3^+$ channel. All the other channels are not observed. Similarly, for resonances below $\text{He}^+(N=4)$ and $\text{He}^+(N=5)$, only the $(2,1)_4^+$ and $(3,1)_5^+$ channels, respectively, were observed. This is consistent with that there is only one dominant $(0,1)_2^+$ channel below $\text{He}^+(N=2)$. Since the ground state belongs to the $(0,0)_1^+$ $1S^e$ channel, it appears that we have selection rules for photoabsorption: $\Delta A=0$ and $\Delta T=1$. Thus $A=-1$ and 0 states are not easily populated in photoabsorption from the ground state. This approximate selection rule can be qualitatively understood in classical terms as follows. In the ground $1S^e$ state, correlation between the two orbits of the two electrons are such that they are coplanar ($T=0$) but opposite senses so that both electrons can approach the nucleus simultaneously ($A=1$). Upon receiving the angular momentum and energy from the photon, it is easier for one of the electrons to change its orbit to a different orientation such that the two orbits are no longer coplanar ($T=1$), while at the same time the sense of rotation ($A=1$) is maintained. To end up with $A=-1$ states, one of the electrons, after photoabsorption, has to change its sense of rotation. In classical planetary motion, we know that this is much harder than just changing the orientation of the orbit. Thus there is an approximate selection rule for $\Delta A=0$. Of course, this qualitative explanation based upon classical orbits should not be taken too literally since the de Broglie wavelength for each electron is quite long. [The above explanation does not apply to the photoabsorption to $1snp$ $1P^o$ channel where there is no strong radial correlation ($A=0$). This is attributed to the fact that photoabsorption to the $1snp$ $1P^o$ channel occurs mostly in the potential valley rather than near the potential ridge.]

The discussion in the previous paragraph implies that photoabsorption from the metastable $1s2s$ $3S^e$ state of He would result in the population of $A=-1$ channels instead of $A=+1$ channels. For example, channels such as $(0,1)_2^-$, $(1,1)_3^-$, and $(2,1)_4^-$ will be strongly populated by photoabsorption from $1s2s$ $3S^e$, while channels such as $(1,0)_2^+$, $(2,0)_3^+$, and $(3,0)_4^+$ will only be weakly populated.²⁰ This means that the lowest resonance state below each threshold, such as $2(1,0)_2^+$, $3(2,0)_3^+$, and $4(3,0)_4^+$ (recall that these states are "designated" as $2s2p$, $3s3p$, and $4s4p$ $3P^o$ according to the independent-particle model) will not be excited by photoabsorption from $1s2s$ $3S^e$, or if excited at all, will be very weak. This also implies an interesting consequence on the Wannier threshold law for the double photoionization of He from $1s2s$ $3S^e$ state. Because the final states have $A=-1$, the Wannier threshold law should have the exponent $m=3.668$ instead of the original $m=1.056$.²¹ Furthermore, the energy partition between the two electrons should show a sharp dip when the two electrons come out with identical energies. On the other hand, the angular correlation still maintains a peak at $\theta_{12}=\pi$. All these predictions are still to be confirmed by experiments.

For electron-atom collisions, such as $e^- + \text{H}$ and $e^- + \text{He}^+$, excitation cross sections depend on the strength of coupling terms among the channels. This requires the evaluation of P matrix, where $P_{\mu\nu} = \langle \Phi_\mu | (d/dR) | \Phi_\nu \rangle$. Although the systematics of P -matrix elements are still rudimentary, existing evidence indicates that P -matrix elements are large for the pair of channels where $\Delta N = 1$, $\Delta K = 1$, $\Delta T = 0$, and $\Delta A = 0$. [These rules are easily deduced from studying the correlation patterns of $(K, T)_N^A$ channels.] Coupling between channels within the same N manifold is small, although to achieve this goal diabatic states are preferred. Well-defined procedures are now available¹⁶ to obtain such diabatic states. Additional study is needed to give a better assessment of the relative strength of coupling terms. If coupling strength to a certain class of channels (e.g., $K < 0$ and/or $A = 0$ channels) is small, these channels might be neglected in future coupled-state calculations. This is definitely desirable, since the number of channels for large N ($N \geq 4$) is large, a conventional close-coupling calculation will become prohibitively difficult because of the large number of channels that have to be included. Close-coupling calculations²² for e -H scattering near $\text{H}(n=2)$ and $\text{H}(n=3)$ thresholds indicated that only $+$ channels are predominantly excited. Thus it appears desirable to perform coupled-channel calculations in hyperspherical coordinates to test the possibility of neglecting all $A = -1$ and 0 doubly excited channels.

ACKNOWLEDGMENTS

I gratefully acknowledge the useful discussion with Birte Christensen-Dalsgaard. This work is supported by U.S. Department of Energy, Division of Chemical Sciences and by Alfred P. Sloan Foundation.

APPENDIX A: SURFACE CHARGE DENSITIES FOR $L \neq 0$ STATES

To display surface charge densities on the (α, θ_{12}) plane at a given hyperspherical radius R for nonspherical $L \neq 0$ states, it is necessary to average over the overall rotation of the atom. This is achieved by defining¹⁸

$$\sigma_\mu(R; \alpha, \theta_{12}) = \int \delta(\cos\theta_{12} - \cos\theta'_{12}) \delta(\alpha - \alpha') \times \Phi_\mu(R; \Omega') \Phi_\mu(R; \Omega) d\Omega', \quad (\text{A1})$$

where $\Omega \equiv (\alpha, \hat{r}_1, \hat{r}_2)$. In our calculation, the channel functions are expressed as

$$\Phi_\mu(R; \Omega) = \frac{1}{\sqrt{2}} \sum_{l_1, l_2} N_{l_1, l_2} f_{l_1, l_2}^\mu(R; \alpha) \mathcal{Y}_{l_1, l_2, LM}(\hat{r}_1, \hat{r}_2) + (-1)^{l_1 + l_2 - L + S} f_{l_1, l_2}^\mu \left[R; \frac{\pi}{2} - \alpha \right] \times \mathcal{Y}_{l_2, l_1, LM}(\hat{r}_1, \hat{r}_2), \quad (\text{A2})$$

where the summation is over truncated pairs of (l_1, l_2) and

$$N_{l_1, l_2} = \begin{cases} 1/\sqrt{2}, & l_1 = l_2 \\ 1, & l_1 \neq l_2. \end{cases} \quad (\text{A3})$$

In terms of the identity

$$\delta(\cos\theta_{12} - \cos\theta'_{12}) = \sum_\lambda \frac{2\lambda + 1}{4\pi} P_\lambda(\cos\theta_{12}) P_\lambda(\cos\theta'_{12}) \quad (\text{A4})$$

Eq. (A1) is given by

$$\sigma_\mu(R; \alpha, \theta_{12}) = \sum_{l_1, l_2} \sum_{l'_1, l'_2} \sum_\lambda \left[\frac{2\lambda + 1}{4\pi} \right] f_{l_1, l_2}^\mu(R; \alpha) f_{l'_1, l'_2}^\mu(R; \alpha) P_\lambda(\cos\theta_{12}) \langle l_1 l_2 L | P_\lambda(\cos\theta'_{12}) | l'_1 l'_2 L \rangle + (-1)^{l'_1 + l'_2 - L + S} f_{l_1, l_2}^\mu(R; \alpha) f_{l'_1, l'_2}^\mu \left[R; \frac{\pi}{2} - \alpha \right] P_\lambda(\cos\theta_{12}) \langle l_1 l_2 L | P_\lambda(\cos\theta'_{12}) | l'_2 l'_1 L \rangle, \quad (\text{A5})$$

where

$$\langle l_1 l_2 L | P_\lambda(\cos\theta_{12}) | l'_1 l'_2 L \rangle = \int \mathcal{Y}_{l_1, l_2, LM}^*(\hat{r}_1, \hat{r}_2) P_\lambda(\cos\theta_{12}) \mathcal{Y}_{l'_1, l'_2, LM}(\hat{r}_1, \hat{r}_2) d\hat{r}_1 d\hat{r}_2 \quad (\text{A6})$$

is the standard F_λ integral of Seaton and Percival.²³

APPENDIX B: COMPARISON OF $(K, T)^A$ QUANTUM NUMBERS WITH THE CLASSIFICATION OF HELIUM DOUBLY EXCITED STATES BELOW $N = 3$ OF LIPSKY *et al.*

Doubly excited states of helium below $N = 2$ and $N = 3$ have been classified into different channels according to the calculated quantum defects by Lipsky *et al.*¹¹ Due to the lack of physically meaningful interpretation of correlations, these channels were named simply as a, b, c, \dots . In Table I, we show the proper $(K, T)^A$ designation for each of the channels labeled by Lipsky *et al.*

TABLE I. Comparison of $(K, T)^A$ quantum numbers with the classification of Lipsky *et al.* (Ref. 11) for doubly excited states of helium below $N=2$ and $N=3$. The first column is the notation used in Ref. 11, and the subsequent columns are from the present classification scheme.

Resonances below $N=2$								
	$^1S^e$	$^3S^e$	$^1P^o$	$^3P^o$	$^1D^e$	$^3D^e$	$^1F^o$	$^3F^o$
				$\pi=(-1)^L$				
<i>a</i>	(1,0) ⁺	(1,0) ⁻	(0,1) ⁺	(1,0) ⁺	(1,0) ⁺	(1,0) ⁻	(1,0) ⁰	(1,0) ⁰
<i>b</i>	(-1,0) ⁺	(-1,0) ⁻	(1,0) ⁻	(0,1) ⁻	(0,1) ⁰	(0,1) ⁰	(0,1) ⁰	(0,1) ⁰
<i>c</i>			(-1,0) ⁰	(-1,0) ⁻	(-1,0) ⁰	(-1,0) ⁰	(-1,0) ⁰	(-1,0) ⁰
Resonances below $N=2$								
			$^3P^e$	$^1P^e$	$^3D^o$	$^1D^o$	$^3F^e$	$^1F^e$
<i>a</i>			(0,1) ⁺	(0,1) ⁻	(0,1) ⁰	(0,1) ⁰	(0,1) ⁰	(0,1) ⁰
Resonances below $N=3$								
	$^1S^e$	$^3S^e$	$^1P^o$	$^3P^o$	$^1D^e$	$^3D^e$	$^1F^o$	$^3F^o$
				$\pi=(-1)^L$				
<i>a</i>	(2,0) ⁺	(2,0) ⁻	(1,1) ⁺	(2,0) ⁺	(2,0) ⁺	(1,1) ⁺	(1,1) ⁺	(2,0) ⁺
<i>b</i>	(0,0) ⁺	(0,0) ⁻	(2,0) ⁻	(0,0) ⁺	(0,2) ⁺	(2,0) ⁻	(2,0) ⁻	(1,1) ⁻
<i>c</i>	(-2,0) ⁺	(-2,0) ⁻	(-1,1) ⁺	(1,1) ⁻	(0,0) ⁺	(0,2) ⁻	(0,2) ⁰	(0,2) ⁰
<i>d</i>			(0,0) ⁻	(-1,1) ⁻	(1,1) ⁻	(0,0) ⁻	(0,0) ⁰	(0,0) ⁰
<i>e</i>			(-2,0) ⁰	(-2,0) ⁰	(-1,1) ⁰	(-1,1) ⁰	(-1,1) ⁰	(-1,1) ⁰
<i>f</i>					(-2,0) ⁰	(-2,0) ⁰	(-2,0) ⁰	(-2,0) ⁰
Resonances below $N=3$								
			$^3P^e$	$^1P^e$	$^3D^o$	$^1D^o$	$^3F^e$	$^1F^e$
<i>a</i>			(1,1) ⁺	(1,1) ⁻	(0,2) ⁺	(1,1) ⁺	(1,1) ⁺	(1,1) ⁻
<i>b</i>			(-1,1) ⁺	(-1,1) ⁻	(1,1) ⁻	(0,2) ⁻	(0,2) ⁰	(0,2) ⁰
<i>c</i>					(-1,1) ⁰	(-1,1) ⁰	(-1,1) ⁰	(-1,1) ⁰

¹R. P. Madden and K. Codling, Phys. Rev. Lett. **10**, 516 (1963); Astrophys. J. **141**, 364 (1965).

²J. W. Cooper, U. Fano, and F. Prats, Phys. Rev. Lett. **10**, 518 (1963).

³U. Fano, Rep. Prog. Phys. **46**, 97 (1983), and references therein.

⁴C. D. Lin, Phys. Rev. A **10**, 1986 (1974).

⁵(a) C. D. Lin, Phys. Rev. A **25**, 76 (1982); (b) **26**, 2305 (1982); (c) **27**, 22 (1983); (d) **25**, 1535 (1982).

⁶C. D. Lin and J. H. Macek, Phys. Rev. A (to be published).

⁷D. R. Herrick and O. Sinanoglu, Phys. Rev. A **11**, 97 (1975).

⁸S. Ezra and R. S. Berry, Phys. Rev. A **25**, 1513 (1982).

⁹M. Crane and L. Armstrong, Jr., Phys. Rev. A **26**, 694 (1982); F. Iachello and A. R. P. Rau, Phys. Rev. Lett. **47**, 501 (1981).

¹⁰C. E. Wulfman, Chem. Phys. Lett. **23**, 370 (1973).

¹¹L. Lipsky, R. Anania, and M. J. Conneely, At. Data Nucl. Data Tables **20**, 127 (1977).

¹²C. D. Lin, Phys. Rev. Lett. **51**, 1348 (1983).

¹³(a) D. R. Herrick, Phys. Rev. A **12**, 413 (1975); (b) S. I. Nikitin and V. N. Ostrovsky, J. Phys. B **11**, 1681 (1978); **9**, 3141 (1976).

¹⁴D. R. Herrick and M. E. Kellman, Phys. Rev. A **21**, 418 (1980); D. R. Herrick, M. E. Kellman, and R. D. Poliak, *ibid.*

22, 1517 (1980).

¹⁵C. D. Lin, Phys. Rev. A **23**, 1585 (1981).

¹⁶B. Christensen-Dalsgaard (unpublished).

¹⁷M. Le Dourneuf, S. Watanabe, and L. Pelamourgues (unpublished).

¹⁸J. W. Warner, L. S. Bartell, and S. M. Blinder, Int. J. Quantum Chem. **18**, 921 (1980).

¹⁹Woodruff and J. A. Samson, Phys. Rev. A **25**, 848 (1982).

²⁰Our conclusion here is different from that of C. H. Greene, Phys. Rev. Lett. **44**, 869 (1980), where it was postulated that + channels are populated from $1s2s\ ^3S^e$ by photoabsorption. Close-coupling calculation by V. L. Jacobs and P. G. Burke, J. Phys. B **5**, 2272 (1972), indicates that photoionization from $1s2s\ ^3S^e$ above the $\text{He}^+(n=2)$ threshold populate - channels.

²¹H. Klar and W. Schlecht, J. Phys. B **9**, 1699 (1976); C. H. Greene and A. R. P. Rau, Phys. Rev. Lett. **48**, 533 (1982). This latter paper also stated that double photoionization from $1s2s\ ^3S^e$ would populate + channels, in disagreement with the present conclusion.

²²J. H. Macek and P. G. Burke, Proc. Phys. Soc. London **92**, 351 (1967).

²³I. C. Percival and M. J. Seaton, Proc. Cambridge Philos. Soc. **53**, 654 (1957).